A FRET map of membrane anchors suggests distinct microdomains of heterotrimeric G proteins

Daniel Abankwa* and Horst Vogel

Ecole Polytechnique Fédérale de Lausanne (EPFL), Institut des Sciences et Ingénierie Chimiques, CH-1015 Lausanne, Switzerland
e-mails: d.abankwa@imb.uq.edu.au; horst.vogel@epfl.ch
*Present address: Institute for Molecular Bioscience, University of Queensland, Brisbane, 4072, Australia

Accepted 21 June 2007
Journal of Cell Science 120, 2953-2962 Published by The Company of Biologists 2007
doi:10.1242/jcs.001404

Summary

The standard model of heterotrimeric G protein signaling postulates a dissociation of Gα and Gβγ subunits after activation. We hypothesized that the different combination of lipid-modifications on Gα and Gαβγ subunits directs them into different microdomains. By characterizing rapidly and at high sensitivity 38 fluorescence resonance energy transfer (FRET) pairs of heterotrimeric-G-protein constructs, we defined their microdomains in relation to each other, free from the constraints of the raft/non-raft dualism. We estimated that in a cell ~30% of these membrane-anchored proteins are mostly clustered in 3400-16,200 copies of 30-nm microdomains. We found that the membrane anchors of Gα and Gαβγ subunits of both the $G_{i/o}$ and G_q family co-cluster differently with microdomain markers. Moreover, anchors of the $G\alpha_{i/o}$ and $G\alpha_q$ subunits co-clustered only weakly, whereas constructs that contained the anchors of the corresponding heterotrimers co-clustered considerably, suggesting the existence of at least three types of microdomain. Finally, FRET experiments with full-length heterotrimeric G proteins confirmed that the inactive, heterotrimerized Gα subunit is in microdomains shared by heterotrimers from different subclasses, from where it displaces upon activation into a membrane-anchor- and subclass-specific microdomain.

Supplementary material available online at
http://jcs.biologists.org/cgi/content/full/120/16/2953/DC1

Key words: FRET, Heterotrimeric G protein, Microdomain, Nanodomain, Raft

Introduction

G-protein-coupled receptors (GPCRs) form one of the largest and pharmacologically most important receptor families (Fredriksson et al., 2003). In the canonical signaling pathway, they activate heterotrimeric G proteins, which then dissociate and allow Gα and Gβγ subunits to specifically access effectors on the intracellular side of the plasma membrane (Gilman, 1987). How this specificity is achieved is only partially understood (Hamm, 1998).

Data on G proteins of the Ras-family suggest that differential partitioning into microdomains could explain effector specificity (Voice et al., 1999; Yan et al., 1998). Ras proteins are structurally most divergent at their C-termini, which contain different membrane-anchoring motifs (Prior and Hancock, 2001). This region directs an isoform-specific and, for H-ras and N-ras, also activation-state-specific lateral segregation in microdomains of the plasma membrane (Prior et al., 2003; Rotblat et al., 2004; Roy et al., 2005), which suggests that their microlocalization contributes to specific effector activation. These Ras microdomains have diameters in the range of nanometers and may depend on cholesterol. Additional evidence for microdomains on the outer and inner leaflet of the plasma membrane of living cells has been provided using FRET (Meyer et al., 2006; Sharma et al., 2004; Zacharias et al., 2002), which allows to study molecular interactions and assemblies in the nanometer range in living cells.

The lateral organization of heterotrimeric G proteins, however, is less well characterized. Immunofluorescence data on heterotrimeric G proteins have shown a subclass-specific colocalization with caveolin and raft markers (Oh and Schnitzer, 2001). Biochemical experiments furthermore revealed different fractionation patterns of active and inactive transducin, the heterotrimeric G protein of photoreception, in detergent-resistant membrane preparations (Nair et al., 2002; Seno et al., 2001). These data suggested that subclass and activation state also influence the membrane organization of heterotrimeric G proteins. However, the correlation of these data with plasma membrane lipid rafts, which were proposed as submicroscopic cholesterol- and sphingolipid-rich dynamic lipid-protein structures in living cells (Simons and Ikonen, 1997), is questionable (Lichtenberg et al., 2005).

Here, we investigated the activation state and subclass dependence of the microdomain localization of heterotrimeric G proteins in living cells. We acquired highly reproducible FRET data on a cytometer, which was much faster than the common microscopy-based approaches. Thus, we were able to analyse a high number of FRET pairs, which allowed us to characterize the overlap of their microdomains by the magnitude of their FRET. Our results show that membrane anchors of Gα and Gαβγ subunits fused to fluorescent proteins cluster differently with distinct microdomain markers. Moreover, fluorescent membrane anchor constructs derived from heterotrimers of the $G_{i/o}$ and G_q subclass cluster together, whereas anchor constructs of the $G\alpha_{i/o}$ and $G\alpha_q$ subunits do not lead to considerable co-clustering. In addition, we

Journal of Cell Science

Journal of Cell Science

determined activation-induced FRET changes of fluorescently tagged full-length heterotrimeric G proteins, which corresponded to those predicted by our clustering data of the membrane anchors. Our data therefore suggest that heterotrimeric G proteins of the $G_{i/o}$ and G_q subclass show a membrane-anchor and activation-state-specific microdomain localization, which may allow these G proteins to specifically and efficiently access effectors.

Results

G-protein-derived membrane anchors direct partial clustering in microdomains of the inner leaflet of the plasma membrane

The submicroscopic clustering of appropriately labelled proteins in microdomains can be studied by analysing the dependence of FRET on the expression level of these proteins (Meyer et al., 2006). Here, by using a calibrated flow cytometer, we analysed rapidly and at high sensitivity 38 monomeric cyan fluorescent protein (mCFP) and monomeric yellow fluorescent protein (mCit) FRET pairs, which were either heterotrimeric-G-protein-derived constructs or constructs serving as microdomain markers (Fig. 1A).

HEK293 cells were transiently co-transfected and fluorescence of at least 10^5 cells was measured. Fluorescence intensity of acceptors and donors covered four orders of magnitude, corresponding to the entire range of observable protein expression. We calculated FRET per cell, using an adapted sensitized acceptor-emission method (Gordon et al., 1998). At constant donor-acceptor ratio of 1:1, FRET efficiencies increased with increasing acceptor concentrations towards a maximal value, E_{max} (Fig. 1D), which we determined as a free fit parameter in equation 1 (see Materials and Methods). Randomly distributed fluorophores in the bulk membrane would amount to less than 5-10% FRET (Fig. 1D left, dashed line) (Wolber and Hudson, 1979) at concentrations where we often observed $E_{max}\approx30\%$ (Fig. 1E, Fig. 4C, Fig. 5A), indicating clustering in microdomains. Supposing that E_{max} is reached at the most dense cubic packing of the

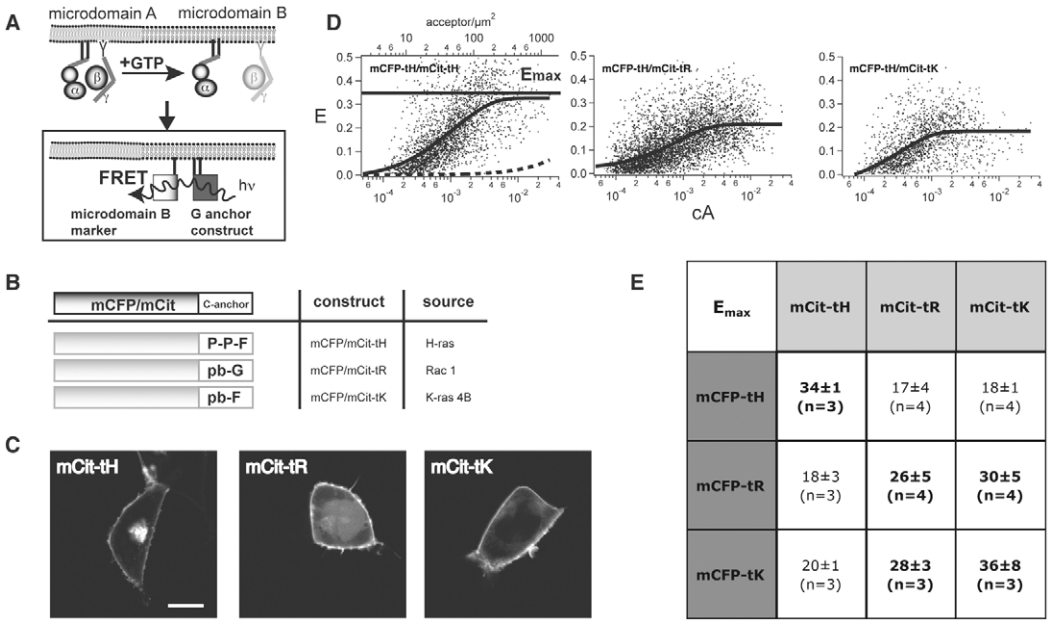

E_{max}	mCit-tH	mCit-tR	mCit-tK
mCFP-tH	**34±1 (n=3)**	17±4 (n=4)	18±1 (n=4)
mCFP-tR	18±3 (n=3)	**26±5 (n=4)**	**30±5 (n=4)**
mCFP-tK	20±1 (n=3)	**28±3 (n=3)**	**36±8 (n=3)**

Fig. 1. Analysis of FRET on the cell membrane demonstrates the distinct levels of co-clustering of microdomain markers. (A) Illustration of our reductionistic approach to study activation-state-dependent microdomain localization of heterotrimeric G proteins. (Top) Activation followed by dissociation of the heterotrimer leads to a separation of Gα and Gβγ subunits. (Bottom) Only the lipid anchors of inactive heterotrimer and active Gα were fused to fluorescent proteins, and the microdomain localization of these G-protein-anchor constructs was studied in relation to microdomain markers (see B and C) using FRET between mCFP as a donor and mCit as an acceptor. (B) Schematic representation of microdomain markers with their lipid anchors. P, palmitoyl; G, geranylgeranyl; F, farnesyl; pb, polybasic sequence. Source refers to the proteins from which targeting sequences were derived. (C) Subcellular localization of microdomain markers imaged by confocal microscopy. All constructs were predominantly localized to the plasma membrane, with minor labeling of internal membranes or, in the case of the Rac1-derived construct, nuclear labeling. Only the mCit constructs are representatively shown. Bars, 10 µm. (D) By plotting the FRET efficiency (E) against the normalized acceptor surface concentration (cA) at a constant donor mole fraction (x_D=0.50±0.17), we obtained information about the clustering of donor and acceptor fluorophores. A random distribution of fluorophores (Wolber and Hudson, 1979) cannot describe our data (left, hashed curve). We found that the FRET efficiencies increased after a cA offset towards a plateau value E_{max} (indicated by solid horizontal line in the left plot). We therefore adapted the double exponential function of Wolber and Hudson (Wolber and Hudson, 1979), further taking the cA offset and the maximum efficiency E_{max} into account. This lead to fits which described all of our FRET data adequately (from left to right, χ^2: 22.6, 25.3 and 9.7). Each datapoint was calculated on a single cell. Representative examples of indicated FRET pairs are shown. (E) The E_{max} matrix of microdomain-marker FRET pairs. FRET values of mCFP-tH/mCit-tH and mCFP-tK/mCit-tK are significantly higher (bold) than those of tH-polybasic pairs (P<0.001 or P<0.05, respectively, 2-tailed Student's t-test). No significant differences were found for consistently high mCFP-polybasic/mCit-polybasic sequence pairs (bold). E_{max} values are given in percent ± s.d.; n, number of independent experiments.

Journal of Cell Science

constructs (modelled as cylinders with a diameter of 3.4 nm), a local concentration of 87,000 fluorophores/μm^2 was estimated. However, E_{max} was already reached at 200-500 acceptor molecules/μm^2 (Fig. 1D left; supplementary material Fig. S1A), implying that fluorophores would be concentrated 87 to 218 times in such microdomains. We can furthermore assume that E_{max} is composed of FRET from microdomains and the bulk of the membrane. Thus, we can calculate the fraction of fluorophores in microdomains (supplementary material Fig. S1B), using equation 2 (see Materials and Methods). At a typical value of E_{max}=30% (Fig. 1E, Fig. 3C, Fig. 4C, Fig. 5A) approximately 26-34% of the membrane-anchored fluorophores were estimated to be in microdomains. This is in very good agreement with FRET data of GPI-anchored proteins on the exoleaflet (Sharma et al., 2004) and electron microscopy (EM) data from the minimal membrane anchor of H-ras fused to GFP on the inner leaflet of the plasma membrane (Plowman et al., 2005), which were both in a minor fraction of 20-40% in nanoclusters. Moreover, using a typical domain size of 30 nm diameter (supplementary material Fig. S1C) and the cell surface divided by the above concentration factors as an estimate for the total microdomain area, we can calculate 3400 to 16,200 microdomains per cell (or 6.5-16/μm^2).

FRET characterizes the lateral segregation of microdomain markers

The dual-palmitoyl–farnesyl membrane anchor of H-Ras was shown to cluster cholesterol dependently in nanometer-sized microdomains, whereas the polybasic sequence of the farnesyl membrane anchor of K-ras 4B (hereafter K-ras) clustered cholesterol independently (Plowman et al., 2005; Prior et al., 2003). Moreover, these membrane anchors, abbreviated tH and tK, for tail of H-Ras and K-ras 4B, respectively, clustered in non-overlapping microdomains (Prior et al., 2003). We therefore fused them to mCFP or mCit in order to generate microdomain markers for different microdomains (Fig. 1B,C). To expand the range of membrane anchors, the targeting sequence of Rac-1 (hereafter abbreviated tR) was chosen to construct another microdomain marker (Fig. 1B,C). This marker contains a polybasic sequence similar to that of K-ras and a geranylgeranyl moiety. Because of the common polybasic sequence, we expected it to also have similar lateral segregation properties as the K-ras-derived marker. We found high E_{max} values above 25% FRET efficiency for mCFP-tH/mCit-tH and mCFP-polybasic/mCit-polybasic FRET pairs (Fig. 1E, bold), consistent with the nanoclustering found by EM analysis (Plowman et al., 2005; Prior et al., 2003). However, E_{max} values of the tH/polybasic pairs were significantly smaller (Fig. 1E, non-bold values), but still above the 5-10% of randomly distributed fluorophores, suggesting some co-clustering in HEK293 cells. However, other FRET pairs (Fig. 3C and Fig. 4C) had E_{max} values close to this theoretical minimum, which demonstrates that we were able to detect with our method the full dynamic range, from non-clustered to highly clustered states.

In summary, a high magnitude of $E_{max} \approx 35\%$ correlated with the nanoclustering of tH or tK found by the EM analysis (Plowman et al., 2005; Prior et al., 2003), whereas values close to the theoretically possible FRET efficiency of randomly distributed fluorophores of 5-10% suggest no clustering. Our FRET values allowed us to detect statistically significant differences over a dynamic range of 25%-increments of E_{max}, which may represent changes in the clustering state. Details on the clustering state cannot be given.

FRET imaging and FRET assays for FRET from internal membranes validate the cytometer approach

To confirm that our FRET predominantly originates from the plasma membrane, we employed sensitized acceptor-emission FRET imaging that allowed us to analyse signals from the plasma membrane only (Fig. 2). Consistent with the predominant localization of the constructs on the plasma membrane, we found FRET levels (Fig. 2; supplementary material Fig. S2A) that were very similar to those measured on the cytometer (Fig. 1E).

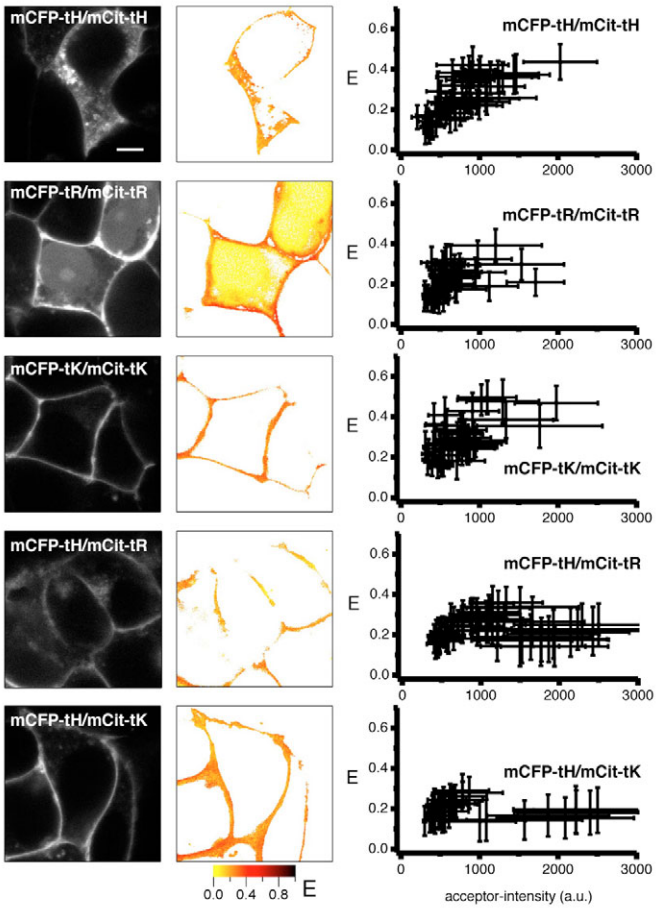

Fig. 2. Sensitized acceptor emission FRET imaging confirms the distinct FRET levels on the plasma membrane. Left to right: FRET-channel images, FRET-efficiency images and dependencies of the FRET efficiency of indicated FRET pairs on the acceptor intensity, corresponding to approximately 500-2000 acceptors/μm^2. Each datapoint was calculated on one region of interest on plasma membranes with donor mole fractions of x_D=0.5±0.17 were analysed. Note that for mCFP-tH/mCit-tH the FRET originating from putative internal membranes show similar values as that originating from the plasma membrane. Consistent with the negligible FRET from soluble fluorophores at these concentrations (supplementary material Fig. S2E), FRET from the nucleus is close to zero for mCFP-tR/mCit-tR. Bars, 5 μm.

Journal of Cell Science

In addition, we developed a quantitative FRET assay for FRET from internal membranes, to determine the FRET contribution from internal membranes that were also populated by our constructs, albeit to a minor extent (e.g. Fig. 1C). We co-expressed each of our constructs with a geranylgeranylated FRET partner (supplementary material Fig. S2B), which binds to all major internal membranes (Goodwin et al., 2005; Rocks et al., 2005; Silvius et al., 2006), and analysed them in the same way as the pairs of the microdomain marker. This assay revealed that, at high expression levels of acceptor, less than 10% FRET efficiency was reached (supplementary material Fig. S2C,D), which is also consistent with our FRET-imaging data. In addition, any contribution from soluble fluorophores in the cytoplasm or nucleoplasm was negligible (supplementary material Fig. S2E).

Membrane-targeting sequences of $G\alpha_{i/o}$ and the $G\alpha_{i/o}\beta\gamma$ heterotrimer direct localization to different microdomains

The standard model of heterotrimeric G protein signaling postulates a dissociation of Gα and Gβγ subunits after receptor activation. We hypothesized that heterotrimer, Gα and Gβγ subunits localize to different microdomains because of their different lipid modifications.

In order to describe the microdomain localization of heterotrimer and Gα subunit, we started with a reductionistic approach (Fig. 1A). We fused the membrane-anchoring sequences of active $G\alpha_{i/o}$ (N_{i2}) or inactive $G\alpha_{i/o}\beta\gamma$ ($N_{i2}C\gamma$) subunits to fluorescent proteins (Fig. 3A). These constructs localized predominantly to the plasma membrane (Fig. 3B) and allowed us to determine their microlocalization in relation to the fluorescent microdomain markers by whole-cell fluorescence measurements.

Next, we characterized the microlocalization of $G\alpha_{i/o}$ membrane anchors. Comparison of the E_{max} values of the FRET pairs of N_{i2}-mCFP and microdomain marker (or -mCit) revealed a characteristic set of E_{max} values for the $G\alpha_{i/o}$ anchor, with higher FRET values for markers that contain polybasic sequences, than for tH (Fig. 3C first column). The E_{max} values, again, reflect the differential co-clustering or the microdomain overlap of microdomain markers and the heterotrimeric-G-protein-derived membrane anchor constructs. We called the set of E_{max} values with the microdomain markers a FRET vector (e.g. any column in Fig. 3C), as it defines the position of the heterotrimeric-G-protein-derived construct in a coordinate system defined by the three microdomain markers.

The FRET vectors of the $G\alpha_{i/o}$-derived anchor construct (Fig. 3A,C first and third column) was mainly associated with the lipid modifications, as we verified by exchanging the membrane-targeting sequence of $G\alpha_{i2}$ with that of Lyn-kinase, which also directs a myristoylation and palmitoylation (Fig. 3A,C second column). Comparison of FRET vectors of $G\alpha_{i/o}$-anchor constructs (Fig. 3A and C column 1-3) with those of $G\alpha_{i/o}\beta\gamma$ constructs (Fig. 3A,C fourth column) revealed that the FRET vectors are different. The E_{max} value of $N_{i2}C\gamma$-mCit/mCFP-tH is significantly larger, and the E_{max} value of $N_{i2}C\gamma$-mCit/mCFP-tR is significantly smaller, than the corresponding $G\alpha_{i/o}$-anchor construct values (Fig. 3C,D). Again, FRET imaging confirmed these relations and the FRET levels on the plasma membrane (supplementary material Fig. S2A). In conclusion, the different FRET vectors of $G\alpha_{i/o}$ and cognate anchor constructs of heterotrimeric G proteins imply that the $G\alpha_{i/o}$ subunit has a different microlocation after activation/dissociation, if the lipid anchors predominantly determine the microdomain localization.

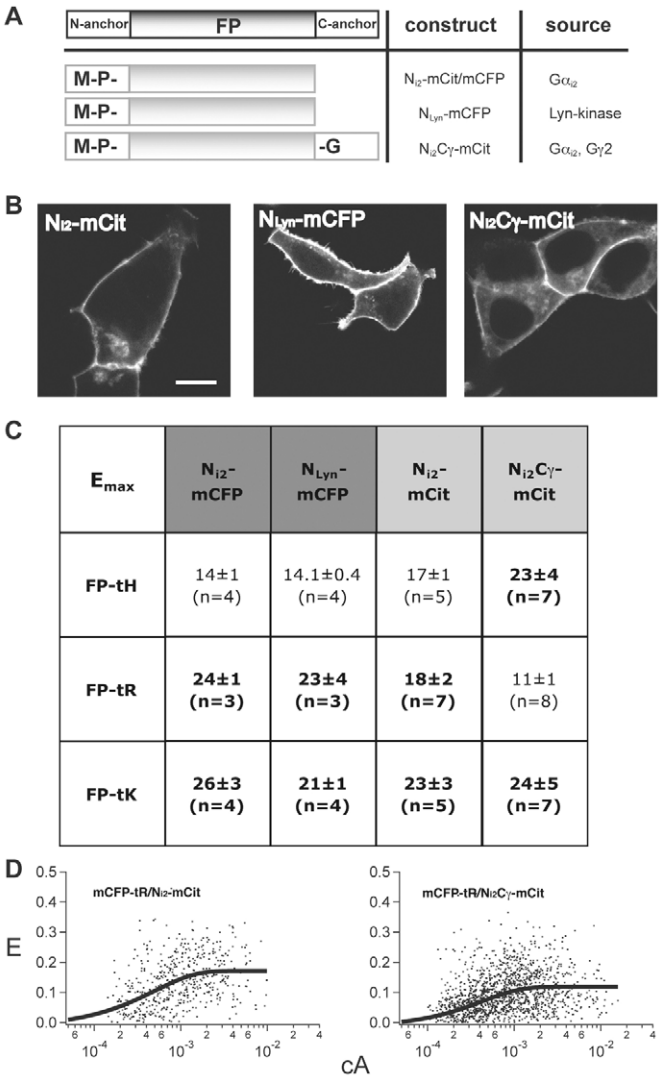

Fig. 3. The $G_{i/o}$ protein anchor construct FRET vector is used to characterize $G\alpha_{i/o}$ and $G\alpha_{i/o}\beta\gamma$ microlocalizations. (A) Schematic representation of heterotrimeric $G_{i/o}$ protein anchor constructs. M, myristoyl; P, palmitoyl; G, geranylgeranyl; FP, fluorescent protein (i.e. either mCFP or mCit). Source refers to the proteins from which targeting sequences were derived. (B) The subcellular localization of $G_{i/o}$-anchor constructs was imaged by confocal microscopy. Bar, 10 μm. (C) The FRET vectors show the E_{max} values of pairs of $G_{i/o}$ anchor constructs and microdomain markers. Column headings give names of G-protein-anchor constructs, row headings give co-expressed microdomain markers. The E_{max} values are given in % ± s.d.; *n,* number of independent experiments. The value for $N_{i2}C\gamma$-mCit/mCFP-tH is significantly larger than the $G\alpha_{i/o}$-anchor construct/FP-tH pairs ($P<0.01$, 2-tailed Student's *t*-test), whereas the value for $N_{i2}C\gamma$-mCit/mCFP-tR is significantly smaller than that for the $G\alpha_{i/o}$-anchor construct/FP-tR pairs ($P<0.001$, 2-tailed Student's *t*-test). (D) Plots of the FRET efficiency (E) against the normalized acceptor surface concentration (cA) at a constant donor mole fraction of indicated FRET pairs with fitted curves as described (from left to right, χ^2: 3.1 and 6.2).

Lipid anchors of $G\alpha_q$ and $G\alpha_q\beta\gamma$ also localize to different microdomains, suggesting that $G\alpha$ and $G\alpha\beta\gamma$ generally localize to different microlocations

In the next step, we tested, whether these conclusions also apply for the membrane anchors of the G_q subclass of heterotrimeric G proteins. An analogous set of constructs was created using the membrane-targeting sequence of $G\alpha_q$ that becomes dually palmitoylated in the native protein. Unfortunately, this sequence alone is not sufficient to confer membrane localization of the protein, which remains in the cytoplasm (Evanko et al., 2000) (and data not shown). However, our results with the $G\alpha_{i/o}$- and Lyn-kinase-derived constructs suggested that the microlocalization is primarily governed by the lipid anchors. Consequently, we used the similarly dually palmitoylated sequence from GAP-43 ($N_{GAP\text{-}43}$), which was sufficient for plasma membrane trafficking (Fig. 4A,B), as a surrogate. The FRET vector of this construct ($N_{GAP\text{-}43}$-mCFP) was again markedly different from the one of the corresponding heterotrimer construct, $N_{GAP\text{-}43}C\gamma$-mCFP (Fig. 4D,C compare column 1 with 2).

We further validated the use of the membrane anchor of GAP-43, by creating a heterotrimer construct that combined the $G\alpha_q$ N-terminal sequence with the $G\gamma2$-derived C-terminal geranylgeranylation site. Consistent with data on plasma membrane trafficking of heterotrimeric G protein (Michaelson et al., 2002), which also suggest two plasma-membrane-targeting signals, the resulting $N_qC\gamma$-mCit localized predominantly to the plasma membrane (Fig. 4A). Whereas the FRET vector of this construct was very similar to the one of $N_{GAP\text{-}43}C\gamma$-mCFP, the E_{max} of $N_qC\gamma$-mCit/mCFP-tR was ~50% smaller than the E_{max} of $N_{GAP\text{-}43}C\gamma$-mCFP/mCFP-tR (Fig. 4C, last two columns).

We propose that the extended stretch of basic residues on one side of the α-helix of the $G\alpha_q$-derived peptide is responsible for this difference (Fig. 4E). However, the E_{max} of the two $G\alpha_q\beta\gamma$ anchor constructs ($N_{GAP\text{-}43}C\gamma$-mCFP/$N_qC\gamma$-mCit; Fig. 5A, dark grey area on the right) was as high as the one of mCFP-tH/mCit-tH or mCFP-tK/mCit-tK (Fig. 1E), indicating that they, nevertheless, considerably co-microlocalize. In summary, these data suggest that $G\alpha_q$ localizes to a different microdomain than its heterotrimer. Again, lipid anchors predominantly determine their microlocalization, which can be modulated by the surrounding amino acids that may contact the membrane. Taking also into account our results with the $G_{i/o}$ anchor construct, we conclude that monomeric Gα protein and the heterotrimer generally localize to different microdomains.

FRET data of membrane anchors suggest that $G\alpha_{i/o}\beta\gamma$ and $G\alpha_q\beta\gamma$ co-microlocalize considerably, whereas $G\alpha_{i/o}$ and $G\alpha_q$ do not

In addition to the anchor constructs of the G_q heterotrimer, we compared directly the microdomain overlap of the anchor constructs of the G_q and $G_{i/o}$ heterotrimers. Consistent with the

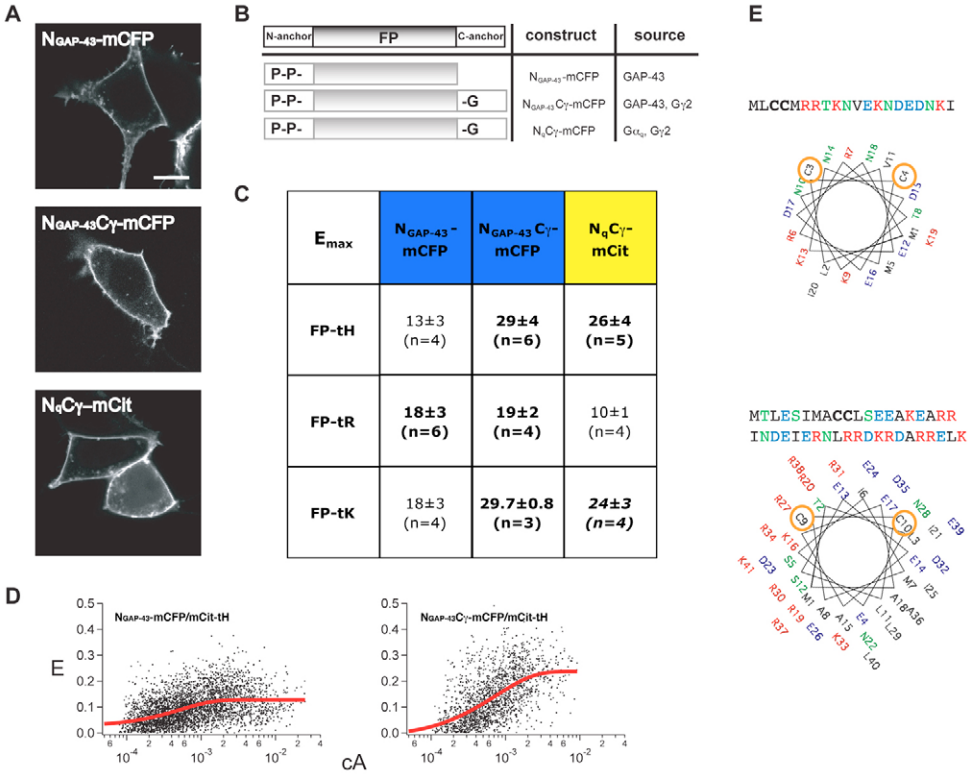

Fig. 4. FRET data of the anchor constructs indicate that $G\alpha_q$ and $G\alpha_q\beta\gamma$ localize to different microdomains. (A) Subcellular localization of G_q-anchor constructs imaged by confocal microscopy revealed predominant plasma membrane labeling. Bar, 10 μm. (B) Schematic representation of constructs of heterotrimeric G_q protein anchor constructs. Abbreviations as in Fig. 3. (C) The FRET vectors show E_{max} values of G_q-anchor construct (blue and yellow column headings highlight mCFP- and mCit-labeled constructs, respectively) and microdomain markers (rows) pairs. The E_{max} values are given in percent with standard deviations and number of independent experiments, n, in brackets. Differences between bold and regular typed values in one row are significant (P<0.01, 2-tailed Student's t-test), however, the P value of $N_qC\gamma$-mCit /mCFP-tK (bold italics) versus $N_{GAP\text{-}43}$-mCFP/mCFP-tK is, P<0.05. (D) Plots of the FRET efficiency (E) against the normalized acceptor surface concentration (cA) at a constant donor mole fraction of indicated FRET pairs with fitted curves as described (from left to right, χ^2: 11.0; 10.3). (E) Since the crystal structures of heterotrimeric G-protein α subunits show a α-helical conformation for their N-terminus (Sprang, 1997), we compared the GAP-43- and $G\alpha_q$-derived targeting sequences in helical wheel projections. These show that the first 20 amino acids of GAP-43 (top) and the first 41 amino acids of $G\alpha_q$ (bottom) that were used for the two $G\alpha_q\beta\gamma$-anchor constructs reveal a more expanded stretch of amino acids with basic side chains (red) on one side of the $G\alpha_q$ helix compared with the GAP-43 helix. These amphipathic helices might modify their microlocalization, which is primarily directed by palmitoylation (sites are encircled in orange; green, acidic side chains; blue, polar side chains).

A

E_{max}	N_{i2}-mCit	$N_{i2}C\gamma$-mCit	$N_qC\gamma$-mCit
N_{i2}-mCFP	**28±5 (n=3)**	n.d.	**25±5 (n=3)**
N_{GAP-43}-mCFP	17±2 (n=3)	11±1 (n=3)	13,8±0,6 (n=3)
$N_{GAP-43}C\gamma$-mCFP	17±2 (n=3)	**30±5 (n=4)**	**34±4 (n=4)**

B

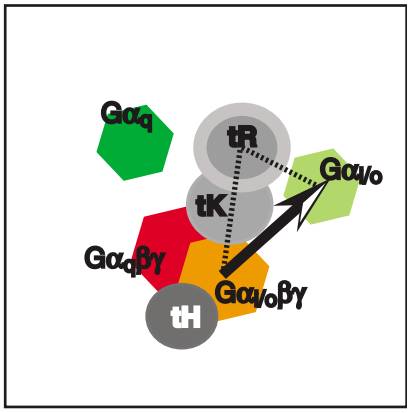

Fig. 5. (A) The direct comparison of G-protein-anchor FRET pairs suggests that $G\alpha_q\beta\gamma$ and $G\alpha_{i/o}\beta\gamma$ share the same microdomain, whereas $G\alpha_{i/o}$ and $G\alpha_q$ do not. The E_{max} values are given in % ± s.d.; *n*, number of independent experiments. E_{max} values of heterotrimer construct FRET pairs are not significantly different (dark grey), whereas the values of Gα construct FRET pairs N_{i2}-mCFP/N_{i2}-mCit and N_{GAP-43}-mCFP/N_{i2}-mCit (light grey) are significantly different ($P<0.05$, 2-tailed Student's *t*-test). Blue and yellow column headings highlight mCFP- and mCit-labeled constructs, respectively. (B) The FRET map of heterotrimeric G-protein microdomains based on the results of their membrane anchors. This scheme is based on the E_{max} relationships, where a high E_{max} value relates to a large overlap of the microdomains or a higher probability of the respective molecules to co-cluster. As an example, the arrow shows how the $G\alpha_{i/o}$ subunit displaces after activation. Its starting microdomain has a lesser 'proximity' to the tR–microdomain-marker (low FRET), than the destination microdomain of active $G\alpha_{i/o}$ (high FRET). Thus, activation results in an increase of FRET for the FRET pair $G\alpha_{i/o}$-construct/tR (Fig. 6C).

very similar FRET vectors of the heterotrimer anchor constructs that indicated similar lateral segregation (Fig. 3C, Fig. 4C), we found a high E_{max} for $N_{GAP-43}C\gamma$-mCFP/$N_{i2}C\gamma$-mCit (Fig. 5A, dark grey area on the right). Therefore, G_q and $G_{i/o}$ heterotrimers may also co-cluster considerably. By contrast, comparison of the FRET values of N_{GAP-43}-mCFP/N_{i2}-mCit and N_{i2}-mCFP/N_{i2}-mCit, suggested that $G\alpha_q$ and $G\alpha_{i/o}$ do not extensively co-cluster (Fig. 5A, light grey area in the middle), as already suggested by their different FRET vectors (Fig. 3C, Fig. 4C).

How do membrane anchors of Gα and Gαβγ subunits from different subclasses microlocalize relative to each other? We generally found low E_{max} values also between Gα- and Gαβγ-anchors from different subclasses (Fig. 5A, white area), suggesting little co-clustering, similar to the FRET pairs of tH/tR or tH/tK (Fig. 1C). An exception is the comparatively high FRET of N_{i2}-mCFP/$N_qC\gamma$-mCit (Fig. 5A, white area on the left). However, the analogous N_{i2}-mCit/$N_{GAP-43}C\gamma$-mCFP had a significantly smaller FRET value (Fig. 5A), making it hard to draw a definite conclusion on the co-microlocalization of $G\alpha_{i/o}$- and $G\alpha_q\beta\gamma$-derived membrane anchor constructs. We conclude that Gα subunits from the G_q and $G_{i/o}$ subclasses localize to different microdomains, while the Gαβγ heterotrimers localize to microdomains that considerably overlap (Fig. 5B).

Predictable FRET changes of full-length heterotrimeric G proteins after activation confirm their relocalization to different microdomains

So far we have based our conclusions on the microlocalization of heterotrimeric G proteins on FRET between fluorescent proteins targeted with G-protein-derived membrane anchors. This was a necessary reduction for the construction of our FRET map of heterotrimeric G protein membrane anchors (Fig. 5B), which required that the distance of the fluorescent proteins to the inner leaflet is very similar for all constructs. We next tested for activation-induced microdomain relocalization of full-length Gα proteins, which can be deduced from our E_{max} relations (Fig. 3C, Fig. 4C) and can be followed in our FRET map (Fig. 5B). We used a fluorescent protein labelling strategy that has been shown to produce functional heterotrimeric Gα subunits (Leaney et al., 2002). Fluorescent proteins were fused to the N-terminus of $G\alpha_{i2}$ and $G\alpha_o$ subunits, and targeted using the previously employed targeting sequences (Fig. 6A,B). FRET between microdomain markers and full-length G-protein constructs was considerably smaller than for the membrane-anchor-only FRET pairs, probably reflecting higher sterical requirements of the full-length G protein. We therefore decided to use a spectrofluorometer of high sensitivity to detect FRET changes after stimulating cells with the membrane-permeating AlF_4^-, which induces a conformational change in heterotrimeric G proteins that corresponds to the transition state of GTP hydrolysis, resulting in dissociation of Gα from the Gβγ subunit (Sondek et al., 1994). After stimulation of cells with AlF_4^-, we found a relative decrease in FRET for N_{GAP-43}-mCFP-$G\alpha_o$/mCit-tH and N_{GAP-43}-mCFP-$G\alpha_o$/mCit-tK, and no change for N_{GAP-43}-mCFP-$G\alpha_o$/mCit-tR (Fig. 6C). However, FRET increased for N_{i2}-mCit-$G\alpha_{i2}$/mCFP-tR and N_{i2}-mCFP-$G\alpha_o$/mCit-tR. Intriguingly, all of these FRET changes corresponded to the changes expected from the E_{max} relations of the corresponding FRET pairs of the Gα- and heterotrimer-anchor constructs (Fig. 3C, Fig. 4C). Control experiments with the corresponding anchor constructs, showed only small FRET decreases (N_{GAP-43}-mCFP/mCit-tH=–8±1, *n*=3; N_{GAP-43}-mCFP/mCit-tR=–5, *n*=1; N_{i2}-mCit/mCFP-tR=–7±4, *n*=2), which we explain with the rearrangements of endogenous, unlabelled heterotrimeric G proteins in microdomains. In summary, our data of anchor constructs allowed us to predict the FRET changes of the full-length Gα constructs. Moreover, their microdomain relocalization was determined by the membrane anchor and not the subclass of the G protein.

Discussion

Our FRET data on fluorescently tagged heterotrimeric-G-protein-derived membrane anchors and full-length proteins suggest a membrane-anchor-specific lateral segregation of heterotrimeric G proteins in microdomains.

We used a cytometer approach to rapidly characterize our FRET pairs on a whole-cell basis. Nevertheless, the sensitized acceptor-emission FRET efficiencies calculated on plasma membrane signals were in the same range as those obtained by

Journal of Cell Science

Journal of Cell Science

our cytometer approach. Both our cytometer FRET and imaging FRET show more scatter of the data points than a similar FRET-imaging approach, where clustering of a GPCR in microdomains was studied (Meyer et al., 2006). This may be explained by our use of fluorescent proteins, because in the other study a novel labeling method was exploited that allowed precise, exogenous control of the mole fraction of the labelled donor, and facilitated also calibration for the surface concentration. Nevertheless, some variability of their data can be seen, suggesting that cell-to-cell variations account for it. However, the cytometer allowed to observe the entire range of protein expression on a single, continuous scale; this revealed the characteristic trends that allowed highly reproducible fitting.

The good reproducibility of our cytometer-FRET approach has recently been demonstrated because the E_{max} values and E_{max} relations could largely be reproduced in BHK cells and using a different cytometer (D.A., unpublished data). Moreover, a surprisingly high sensitivity could be shown by its ability to detect the influence of individual amino acid exchanges on an 8-dimensional (8 different microdomain marker) lateral segregation FRET vector of H-ras, stressing the potential of this approach (D.A., unpublished data).

The assumptions that allowed us to derive the fraction of our anchor constructs in microdomains are simplistic, but produce numbers that are in striking agreement with those obtained with different methods (Plowman et al., 2005; Sharma et al., 2004). The actual packing of the fluorophores at concentrations where E_{max} was determined may not be the most dense packing. Therefore, the actual FRET efficiency within the microdomain/nanocluster might be smaller we assumed. At the same time, FRET originating from proteins that are not in nanoclusters might be smaller than the assumed 10% efficiency. Altogether, the estimates of proteins in microdomains/nanoclusters might be lower estimates.

In further support of our approach, we analysed our data on the dependence of the FRET efficiency on the donor mole fraction (at constant cA) with a model for FRET in oligomers (D.A. and H.V., unpublished data). Nanoclusters have a weak resemblance to oligomers, in that they contain a characteristic number of proteins (Plowman et al., 2005; Sharma et al., 2004). Intriguingly, we determined three to six proteins in a hypothetical oligomer or nanocluster, which was again in full agreement with the two to seven proteins previously determined for nanoclusters (Plowman et al., 2005; Sharma et al., 2004). Also, our estimate of the absolute number of microdomains (3400-16,200) in a cell is comparable with data from active K-ras where ~46,000 microdomains were calculated (Tian et al., 2007).

Our FRET data correlate very well with the EM-clustering analysis of H- and K-ras membrane anchors (Plowman et al., 2005; Prior et al., 2003), which supports our view that the E_{max} value is a good measure for nanoclustering. The relative differences of the E_{max} values allowed conclusions about the co-clustering of our FRET pairs of anchor constructs. At some variance with the EM analysis (Prior et al., 2003), the E_{max} value of the tH/tK pair suggests some co-clustering in HEK293 cells. FRET analysis may therefore appear more sensitive than EM analysis. However, this comparison cannot easily be made, because the FRET and EM analyses are sensitive for clustering on different, partially overlapping (Hess et al., 2005), length scales, namely 3-10 nm and above 5 nm, for FRET and EM respectively. However, it is possible that low levels of co-clustering cannot be detected using the EM analysis. Alternatively, the protein distribution of tH/tK in HEK293 may not exactly match that of BHK cells. Either way, our dynamic range of E_{max} values remains valid, because other FRET pairs, such as mCFP-tR/N_{i2}Cγ-mCit (Fig. 3C) or mCFP-tR/N_qCγ-mCit (Fig. 4C) show E_{max} values close to the predicted value for randomly distributed donors and acceptors.

Our data of membrane anchors indicate that heterotrimers of different G-protein subclasses reside in microdomains (or nanoclusters) that

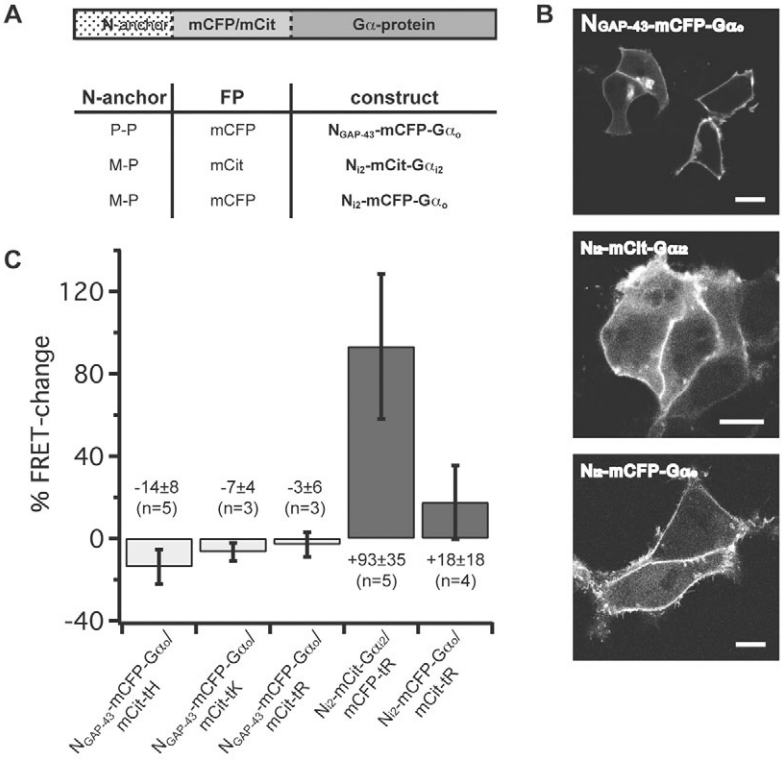

Fig. 6. FRET experiments with full-length heterotrimeric-G-protein constructs confirm displacement of the Gα subunit into another microdomain after activation, as predicted by the FRET vectors of the anchor constructs. (A) Schematic representation of fluorescent full-length heterotrimeric-G-protein constructs. We fused the fluorescent protein (FP) to the N-terminus of the Gα subunits and targeted these fusion constructs using the targeting sequences of the G-protein-anchor constructs. (B) Confocal imaging confirmed that all full-length Gα constructs are predominantly localized to the plasma membrane. Bars, 10 μm. (C) FRET changes were calculated after stimulating cells with AlF_4^- (30 μM, 40 minutes, 22°C). Fluorescence of cells co-expressing indicated full-length G-protein constructs, microdomain markers and in addition unlabelled Gβ1γ2, was measured in a sensitive spectrofluorometer. Numbers at the bars give the average FRET change in percent with standard deviations and number of independent experiments, *n*, in brackets.

Journal of Cell Science

considerably overlap (Fig. 5B). This would allow for the promiscuity of receptor-heterotrimer interactions often observed. However, the membrane-anchor-specific separation of activated Gα-proteins (Fig. 5B), could provide an explanation for a membrane-anchor-specific and subclass-specific (subclassification is to a large extent determined by the N-terminal membrane anchor) use of effector. The membrane-anchor-specific lateral segregation of signaling proteins would support similar observations made for Ras (Prior et al., 2001). Ras data furthermore suggest the existence of at least three types of microdomain (Prior et al., 2003; Roy et al., 2003). This again parallels our results, as we postulate at least three distinct microdomains for $G\alpha_{i/o}$, $G\alpha_q$ and the heterotrimers that are, however, again different from the microdomains labelled by our microdomain markers (Fig. 5B).

The usefulness of membrane-anchor data is validated by a study using single-particle tracking, which revealed very similar diffusion modes for full-length heterotrimeric Gα and Gαβγ constructs, and corresponding membrane anchor constructs (Perez et al., 2006). It furthermore provides an interesting correlation of diffusion data on membrane sheets and FRET data in living cells.

The strongest support for our approach comes from our FRET data on stimulated full-length heterotrimeric G proteins (Fig. 6C). The FRET map summary, derived from membrane anchor data (Fig. 5B), allowed to predict and interpret the results in Fig. 6C, which suggest that heterotrimeric G_o and G_{i2} proteins dissociate to an extent that allows the membrane anchor on Gα to induce a different microdomain for its subunit. This is in line with the standard model of G-protein action, which is supported by several other FRET studies (Azpiazu and Gautam, 2004; Gibson and Gilman, 2006; Janetopoulos et al., 2001), but difficult to reconcile with reports proposing that only $G\alpha_o$ and not $G\alpha_i$ proteins dissociate (Frank et al., 2005).

In search of molecular determinants for the observed microlocalization, we propose that a polybasic sequence in conjunction with an isoprenylation leads to co-clustering. Our data of the Gα constructs indicate that a palmitoyl to myristoyl exchange is sufficient to localize the construct to different microdomains. The trimer constructs, however, have an E_{max} value as high (Fig. 5A, dark grey area on the right) as mCFP-tH/mCit-tH (Fig. 1E) and also the E_{max} values of any pair of the trimer-anchor constructs and tH is very high (Fig. 3C, Fig. 4C). Hence, dual palmitoylation and geranylgeranylation on tH and our constructs $N_{GAP\text{-}43}C\gamma$-mCFP, $N_qC\gamma$-mCFP and myristoyl-palmitoyl-geranylgeranylation on $N_{i2}C\gamma$-mCit do not only look very similar biochemically, but also lead to microlocalization in largely overlapping microdomains.

Interestingly, we observed differences in the clustering of constructs, which mimic the lipid modifications of $G\alpha_q\beta\gamma$. We attributed this to differences in their amino acid sequence and, specifically, to the stretch of basic residues (Fig. 4E). The impact of amino acids, especially of those which surround lipid modifications, on microlocalization was also observed by EM for constructs derived from H-ras (Rotblat et al., 2004) but may now be rationalized on the basis of a recent computational simulation of membrane-bound H-ras (Gorfe et al., 2007). In conclusion, the lipidic membrane anchor predominates microlocalization of heterotrimeric G proteins. However, it cannot be excluded that additional modulating effects by the anchoring peptide, palmitate turnover or masking and unmasking of basic domains or isoprenyl moieties affect microlocalization.

Our results therefore support the revision of the raft hypothesis (Hancock, 2006), which so far only distinguished between cholesterol-dependent raft and cholesterol-independent non-raft microdomains. However, the FRET-map approach exemplified here allows the characterization of several microdomains, thus providing a more powerful alternative to cholesterol-depletion experiments, which are also error prone due to unspecific effects of cholesterol-depleting agents (Shvartsman et al., 2006). Our data support distinct complexes formed by lipid anchors, surrounding amino acids and membrane lipids, which might induce dynamic, partially overlapping nanoscale assemblies, and might also depend on cholesterol. We believe that this revised model is more suitable to explain the lateral segregation of the plethora of membrane-anchoring motifs, which mostly serve specific cell biological purposes (Fivaz and Meyer, 2003) and might quite possibly not only be confined to two types of microdomain. Our relational FRET map approach will allow to address unresolved questions of membrane microdomains of membrane-anchored or membrane-spanning proteins, such as coupling of domains between two leaflets and modulating effects of putatively membrane-interacting amino acids.

Materials and Methods

Molecular cloning

To construct the microdomain markers, the minimal membrane-anchoring sequences of murine H-ras, K-ras 2B, Rac1 or of the G protein Gγ2 subunit were C-terminally fused to mCFP and mCit [A206K mutation (Zhang et al., 2002) of eCFP (Clontech) and the improved YFP citrine (Griesbeck et al., 2001), respectively]. The G-protein-anchor constructs were generated by fusing the anchoring sequences of the murine G protein subunits $G\alpha_{i2}$ and $G\alpha_q$, murine Lyn and human GAP-43 to the N-terminus of fluorescent proteins, which for Gαβγ-anchor constructs contained also the Gγ2 anchor. Full-length heterotrimeric G protein constructs were constructed as described by others (Leaney et al., 2002), but by using the indicated membrane-targeting sequences (see supplementary material Table S1).

Cell culture

Adherent human embryonic kidney (HEK293) cells were grown in Dulbecco's modified Eagle's medium F-12 (Invitrogen), supplemented with 2.2% fetal calf serum. Cells were cultured in plastic flasks (TPP AG, Trasadingen) at 37°C and 5% CO_2. Transfection was done using Effectene transfection reagent (Qiagen).

Fluorescence measurements by flow cytometry

Cells were harvested 2 days after transfection with EDTA (5 mM, pH 7.4) washed with PBS (Sigma) and resuspended in PBS. We used a CyAn ADP flow cytometer (Dako Cytomation) to measure fluorescence of 1×10^5 to 2×10^5 events in the donor (405 nm excitation, 450/50 emission filter), acceptor (488 nm excitation, 530/40 emission filter) and FRET (405 nm excitation, 530/40 emission filter) channels, with detector gains set to accommodate the full range of expression levels. Raw data were imported into IgorPro5 (Wavemetrics) for subsequent data treatment. We calculated the normalized acceptor surface concentration using the equation $cA=N_A/A_{cell}R_0^2$. Therein, N_A is the number of acceptor fluorophores derived from normalizing fluorescence in the acceptor channel with the fluorescence signal of the cellular background. This was conservatively estimated to correspond to 10,000 molecules. This was verified with fluorescent giant unilamellar vesicles of known concentration of fluorophore on their surface (data not shown). A_{cell}, is the surface area of a HEK cell estimated as a sphere with the average diameter of 15.4±2.4 μm (n=70). A fusion construct of mCFP-mCit was used to calibrate for a 1:1 stoichiometry of donor:acceptor (corresponding to x_D=0.5±0.17). We have selected in silico for those cells, with the donor mole fraction of x_D=0.5±0.17 (corresponding to donor:acceptor≈1:1 stoichiometry) and used only this population for subsequent data analysis. FRET was calculated per cell by using an adapted sensitized acceptor-emission method (Gordon et al., 1998), using E(mCFP-mCit)=0.35±0.03 for calibration of the conversion factor G. Dependence of the FRET efficiency E on the normalized acceptor surface concentration cA was fitted, using the following

Journal of Cell Science

descriptive function, which is adapted from the one used by Wolber and Hudson (Wolber and Hudson, 1979):

$$E = E_{max} - [A_1 e^{-k1 \cdot a \cdot (cA+cA_0)} + A_2 e^{-k2 \cdot a \cdot (cA+cA_0)}] , \quad (1)$$

with A_1=0.6322, k_1=3.1871, A_2=0.3678, k_2=0.7515, for $R_c/R_0 \approx 0.7$; using R_0=4.7 nm, the Förster radius of mCFP/mCit, calculated using spectroscopic data of the purified proteins (D.A., unpublished data) and R_c=3.4 nm. R_c was the distance of closest approach of the fluorescent proteins, which was estimated by modeling them as cylinders, of 2.5×4 nm, with the transition dipole moment in its center (Griesbeck et al., 2001; Rosell and Boxer, 2003). Because the relative orientation of the membrane-anchored fluorophores is not known, R_c was calculated as an arbitrarily chosen weighted average of the distances of the dipole moment of three different orientations of the fluorophores. Orientation 1 was side-by-side, $R_c(i)$=2.5 nm, x(i)=0.5; orientation 2 was top-on-bottom, $R_c(ii)$=4 nm, x(ii)=0.25; orientation 3 was edge-on-edge, $R_c(iii)$=4.6 nm, x(iii)=0.25. $R_c = x(i)R_c(i) + x(ii)R_c(ii) + x(iii)R_c(iii)$=3.4 nm. The free fit parameter 'a', the offset on the cA axis 'cA_0' and the maximum efficiency reached at high cA 'E_{max}', resulted from our adaptation.

We calculated the fraction of molecules present in microdomains with the most dense cubic packing was calculated using equation 2:

$$E_{max} = x_{micro}E_{micro} + (1-x_{micro})\, E_{bulk} , \quad (2)$$

with E_{micro}=87% being the efficiency in the microdomains at the most dense packing, calculated with $E=1/(1+(R/R_0)^6)$, using R_0=4.7 nm $R=R_c$=3.4 nm (see supplementary material Fig. S1B for a table of x_{micro}).

Confocal microscopy and sensitized acceptor FRET imaging

HEK293 were plated on coverslips (0.18 mm), overlaid with PBS and imaged using a LSM 510 confocal microscope (Zeiss) equipped with appropriate filtersets for CFP and YFP imaging. FRET was measured as sensitized acceptor emission using the three cube method essentially as described by others (Gordon et al., 1998). Images in donor (excitation 405 nm, emission 470-500 nm), acceptor (excitation 514 nm, emission 530-600 nm) and FRET (excitation 405 nm, emission 530-600 nm) channels were acquired on a Zeiss LSM 510 Meta using a 63× or 100× oil immersion objective, with numerical apertures of 1.4. The acceptor channel was adjusted to a setting corresponding to ~500-2000 acceptors/μm^2, using giant unilamellar vesicles with 1000, 2000 and 4000 FITC/μm^2, and taking into account that the brightness of FITC is ≈3.8 times smaller than of mCit at 514 nm excitation (based on their extinction coefficient and quantum yields). Similar to the cytometer approach, the mCFP-mCit fusion protein was used to calibrate for the FRET efficiency and donor-acceptor stoichiometry. Images were analysed using a custom written procedure in IgorPro5, that performed background subtraction, crosstalk correction, shifting of correlated three-cube-images and, if required, thresholding. FRET was calculated on a pixel-by-pixel basis. Per image, three regions of interest on the plasma membrane were chosen.

Fluorescence measurements on a spectrofluorometer

Fluorescence measurements were done on a SpexFluorolog II (Instrument S.A.) at 1.60 nm excitation-band- and 0.90 nm emission-band passes. Stirred cell suspensions in a quartz cuvette (10×4 mm^2, 1500 μl, Hellma) were excited consecutively at 430 nm and 510 nm, with emission being recorded from 440-600 nm and 520-600 nm, respectively. FRET was determined as 'FR', the sensitized acceptor emission FRET ratio; $FR=F_{AD}/F_A$, where F_{AD} and F_A are the fluorescence of the acceptor in the presence and absence of the donor, respectively. We derived FR from $FR=d_{430}/d_{510}$, given that the recorded sample spectra are: $S_yx(\lambda ex) = a_{\lambda ex}f1(buffer) + b_{\lambda ex}f2(HEK) + c_{\lambda ex}f3(HEK/mCFP) + d_{\lambda ex}f4(HEK/mCit)$, with $S_yx(\lambda ex)$ being the fluorescence signal of y (e.g. acceptor or donor) of the sample containing x (e.g. acceptor and donor) after excitation at λex nm; f1-f2 were the spectra of reference samples as indicated in brackets, recorded by excitation at the indicated wavelengths; coefficients $a_{\lambda ex}$ to $d_{\lambda ex}$ are the fit parameters. The percent FRET change after AlF_4^- treatment (30 μM, 40 min, 22°C) was calculated as: $(FR_{after}-1)/(FR_{before}-1)\times 100-100$.

We thank Andrew Tinker for the kind gift of the parent constructs of the membrane targeted, fluorescent $G\alpha_{i/o}$ proteins, Peter Ulrich for help with programming, Bruno Meyer and Jean-Manuel Segura for valuable discussions, and Ruud Hovius for critical reading of the manuscript. D.A. is grateful to John Hancock for his helpful advice on the manuscript. This work was supported by the Swiss National Science Foundation (NF 4047-057572), the TopNano21 program (projects 5636.2 and 6266.1), and internal grants from the EPFL.

References

Azpiazu, I. and Gautam, N. (2004). A fluorescence resonance energy transfer-based sensor indicates that receptor access to a G protein is unrestricted in a living mammalian cell. *J. Biol. Chem.* **279**, 27709-27718.

Evanko, D. S., Thiyagarajan, M. M. and Wedegaertner, P. B. (2000). Interaction with Gbetagamma is required for membrane targeting and palmitoylation of Galpha(s) and Galpha(q). *J. Biol. Chem.* **275**, 1327-1336.

Fivaz, M. and Meyer, T. (2003). Specific localization and timing in neuronal signal transduction mediated by protein-lipid interactions. *Neuron* **40**, 319-330.

Frank, M., Thumer, L., Lohse, M. J. and Bunemann, M. (2005). G Protein activation without subunit dissociation depends on a G{alpha}(i)-specific region. *J. Biol. Chem.* **280**, 24584-24590.

Fredriksson, R., Lagerstrom, M. C., Lundin, L. G. and Schioth, H. B. (2003). The G-protein-coupled receptors in the human genome form five main families. Phylogenetic analysis, paralogon groups, and fingerprints. *Mol. Pharmacol.* **63**, 1256-1272.

Gibson, S. K. and Gilman, A. G. (2006). Gialpha and Gbeta subunits both define selectivity of G protein activation by alpha2-adrenergic receptors. *Proc. Natl. Acad. Sci. USA* **103**, 212-217.

Gilman, A. G. (1987). G proteins: transducers of receptor-generated signals. *Annu. Rev. Biochem.* **56**, 615-649.

Goodwin, J. S., Drake, K. R., Rogers, C., Wright, L., Lippincott-Schwartz, J., Philips, M. R. and Kenworthy, A. K. (2005). Depalmitoylated Ras traffics to and from the Golgi complex via a nonvesicular pathway. *J. Cell Biol.* **170**, 261-272.

Gordon, G. W., Berry, G., Liang, X. H., Levine, B. and Herman, B. (1998). Quantitative fluorescence resonance energy transfer measurements using fluorescence microscopy. *Biophys. J.* **74**, 2702-2713.

Gorfe, A. A., Bayer, M.-H., Abankwa, D., Hancock, J. F. and McCammon, J. A. (2007). Structure and dynamics of the full-length lipid-modified H-Ras protein in a 1,2-dimyristoylglycero-3-phosphocholine bilayer. *J. Med. Chem.* **50**, 674-684.

Griesbeck, O., Baird, G. S., Campbell, R. E., Zacharias, D. A. and Tsien, R. Y. (2001). Reducing the environmental sensitivity of yellow fluorescent protein. Mechanism and applications. *J. Biol. Chem.* **276**, 29188-29194.

Hamm, H. E. (1998). The many faces of G protein signaling. *J. Biol. Chem.* **273**, 669-672.

Hancock, J. F. (2006). Lipid rafts: contentious only from simplistic standpoints. *Nat. Rev. Mol. Cell Biol.* **7**, 456-462.

Hess, S. T., Kumar, M., Verma, A., Farrington, J., Kenworthy, A. and Zimmerberg, J. (2005). Quantitative electron microscopy and fluorescence spectroscopy of the membrane distribution of influenza hemagglutinin. *J. Cell Biol.* **169**, 965-976.

Janetopoulos, C., Jin, T. and Devreotes, P. (2001). Receptor-mediated activation of heterotrimeric G-proteins in living cells. *Science* **291**, 2408-2411.

Leaney, J. L., Benians, A., Graves, F. M. and Tinker, A. (2002). A novel strategy to engineer functional fluorescent inhibitory G-protein alpha subunits. *J. Biol. Chem.* **277**, 28803-28809.

Lichtenberg, D., Goni, F. M. and Heerklotz, H. (2005). Detergent-resistant membranes should not be identified with membrane rafts. *Trends Biochem. Sci.* **30**, 430-436.

Meyer, B. H., Segura, J. M., Martinez, K. L., Hovius, R., George, N., Johnsson, K. and Vogel, H. (2006). FRET imaging reveals that functional neurokinin-1 receptors are monomeric and reside in membrane microdomains of live cells. *Proc. Natl. Acad. Sci. USA* **103**, 2138-2143.

Michaelson, D., Ahearn, I., Bergo, M., Young, S. and Philips, M. (2002). Membrane trafficking of heterotrimeric G proteins via the endoplasmic reticulum and Golgi. *Mol. Biol. Cell* **13**, 3294-3302.

Nair, K. S., Balasubramanian, N. and Slepak, V. Z. (2002). Signal-dependent translocation of transducin, RGS9-1-Gbeta5L complex, and arrestin to detergent-resistant membrane rafts in photoreceptors. *Curr. Biol.* **12**, 421-425.

Oh, P. and Schnitzer, J. E. (2001). Segregation of heterotrimeric G proteins in cell surface microdomains. G(q) binds caveolin to concentrate in caveolae, whereas G(i) and G(s) target lipid rafts by default. *Mol. Biol. Cell* **12**, 685-698.

Perez, J. B., Segura, J. M., Abankwa, D., Piguet, J., Martinez, K. L. and Vogel, H. (2006). Monitoring the diffusion of single heterotrimeric G proteins in supported cell-membrane sheets reveals their partitioning into microdomains. *J. Mol. Biol.* **363**, 918-930.

Plowman, S. J., Muncke, C., Parton, R. G. and Hancock, J. F. (2005). H-ras, K-ras, and inner plasma membrane raft proteins operate in nanoclusters with differential dependence on the actin cytoskeleton. *Proc. Natl. Acad. Sci. USA* **102**, 15500-15505.

Prior, I. A. and Hancock, J. F. (2001). Compartmentalization of Ras proteins. *J. Cell Sci.* **114**, 1603-1608.

Prior, I. A., Harding, A., Yan, J., Sluimer, J., Parton, R. G. and Hancock, J. F. (2001). GTP-dependent segregation of H-ras from lipid rafts is required for biological activity. *Nat. Cell Biol.* **3**, 368-375.

Prior, I. A., Muncke, C., Parton, R. G. and Hancock, J. F. (2003). Direct visualization of Ras proteins in spatially distinct cell surface microdomains. *J. Cell Biol.* **160**, 165-170.

Rocks, O., Peyker, A., Kahms, M., Verveer, P. J., Koerner, C., Lumbierres, M., Kuhlmann, J., Waldmann, H., Wittinghofer, A. and Bastiaens, P. I. (2005). An acylation cycle regulates localization and activity of palmitoylated Ras isoforms. *Science* **307**, 1746-1752.

Rosell, F. I. and Boxer, S. G. (2003). Polarized absorption spectra of green fluorescent protein single crystals: transition dipole moment directions. *Biochemistry* **42**, 177-183.

Rotblat, B., Prior, I. A., Muncke, C., Parton, R. G., Kloog, Y., Henis, Y. I. and Hancock, J. F. (2004). Three separable domains regulate GTP-dependent association of H-ras with the plasma membrane. *Mol. Cell. Biol.* **24**, 6799-6810.

Roy, A. A., Lemberg, K. E. and Chidiac, P. (2003). Recruitment of RGS2 and RGS4 to the plasma membrane by G proteins and receptors reflects functional interactions. *Mol. Pharmacol.* **64**, 587-593.

Roy, S., Plowman, S., Rotblat, B., Prior, I. A., Muncke, C., Grainger, S., Parton, R. G., Henis, Y. I., Kloog, Y. and Hancock, J. F. (2005). Individual palmitoyl residues serve distinct roles in H-ras trafficking, microlocalization, and signaling. *Mol. Cell. Biol.* **25**, 6722-6733.

Seno, K., Kishimoto, M., Abe, M., Higuchi, Y., Mieda, M., Owada, Y., Yoshiyama, W., Liu, H. and Hayashi, F. (2001). Light- and guanosine 5′-3-O-(thio)triphosphate-sensitive localization of a G protein and its effector on detergent-resistant membrane rafts in rod photoreceptor outer segments. *J. Biol. Chem.* **276**, 20813-20816.

Sharma, P., Varma, R., Sarasij, R. C., Ira, Gousset, K., Krishnamoorthy, G., Rao, M. and Mayor, S. (2004). Nanoscale organization of multiple GPI-anchored proteins in living cell membranes. *Cell* **116**, 577-589.

Shvartsman, D. E., Gutman, O., Tietz, A. and Henis, Y. I. (2006). Cyclodextrins but not compactin inhibit the lateral diffusion of membrane proteins independent of cholesterol. *Traffic* **7**, 917-926.

Silvius, J. R., Bhagatji, P., Leventis, R. and Terrone, D. (2006). K-ras4B and prenylated proteins lacking "second signals" associate dynamically with cellular membranes. *Mol. Biol. Cell* **17**, 192-202.

Simons, K. and Ikonen, E. (1997). Functional rafts in cell membranes. *Nature* **387**, 569-572.

Sondek, J., Lambright, D. G., Noel, J. P., Hamm, H. E. and Sigler, P. B. (1994). GTPase mechanism of Gproteins from the 1.7-A crystal structure of transducin alpha-GDP-AIF-4. *Nature* **372**, 276-279.

Sprang, S. R. (1997). G protein mechanisms: insights from structural analysis. *Annu. Rev. Biochem.* **66**, 639-678.

Tian, T., Harding, A., Inder, K., Plowman, S., Parton, R. G. and Hancock, J. F. (2007). Plasma membrane nanoswitches generate high-fidelity Ras signal transduction. *Nat Cell Biol*. PMID: 17618274.

Voice, J. K., Klemke, R. L., Le, A. and Jackson, J. H. (1999). Four human ras homologs differ in their abilities to activate Raf-1, induce transformation, and stimulate cell motility. *J. Biol. Chem.* **274**, 17164-17170.

Wolber, P. K. and Hudson, B. S. (1979). An analytic solution to the Forster energy transfer problem in two dimensions. *Biophys. J.* **28**, 197-210.

Yan, J., Roy, S., Apolloni, A., Lane, A. and Hancock, J. F. (1998). Ras isoforms vary in their ability to activate Raf-1 and phosphoinositide 3-kinase. *J. Biol. Chem.* **273**, 24052-24056.

Zacharias, D. A., Violin, J. D., Newton, A. C. and Tsien, R. Y. (2002). Partitioning of lipid-modified monomeric GFPs into membrane microdomains of live cells. *Science* **296**, 913-916.

Zhang, J., Campbell, R. E., Ting, A. Y. and Tsien, R. Y. (2002). Creating new fluorescent probes for cell biology. *Nat. Rev. Mol. Cell. Biol.* **3**, 906-918.

Journal of Cell Science